Cell

TREK-1 and Best1 Channels Mediate Fast and Slow Glutamate Release in Astrocytes upon GPCR Activation

Dong Ho Woo,[1,2] Kyung-Seok Han,[1,2] Jae Wan Shim,[3] Bo-Eun Yoon,[1,2] Eunju Kim,[1] Jin Young Bae,[5] Soo-Jin Oh,[1,6] Eun Mi Hwang,[1] Alan D. Marmorstein,[7] Yong Chul Bae,[5] Jae-Yong Park,[1,4,*] and C. Justin Lee[1,2,*]

[1]Center for Neural Science and WCI Center for Functional Connectomics, Korea Institute of Science and Technology, Seoul 136-791, Republic of Korea

[2]Neuroscience Program, University of Science and Technology (UST), Daejeon 305-350, Republic of Korea

[3]Future Convergence Research Division, Korea Institute of Science and Technology and University of Science and Technology, Seoul 136-791, Republic of Korea

[4]Department of Physiology, Institute of Health Sciences, Medical Research Center for Neural Dysfunction, School of Medicine, Gyeongsang National University, Jinju 660-751, Republic of Korea

[5]Department of Oral Anatomy and Neurobiology, BK21, School of Dentistry, Kyungpook National University, Daegu 700-412, Republic of Korea

[6]Department of Cell and Developmental Biology, Dental Research Institute, School of Dentistry, Seoul National University, Seoul 110-749, Republic of Korea

[7]Department of Ophthalmology and Vision Science, College of Medicine and College of Optical Sciences, University of Arizona, Tucson, AZ 85711, USA

*Correspondence: jaeyong@gnu.ac.kr (J.-Y.P.), cjl@kist.re.kr (C.J.L.)

http://dx.doi.org/10.1016/j.cell.2012.09.005

SUMMARY

Astrocytes release glutamate upon activation of various GPCRs to exert important roles in synaptic functions. However, the molecular mechanism of release has been controversial. Here, we report two kinetically distinct modes of nonvesicular, channel-mediated glutamate release. The fast mode requires activation of $G_{\alpha i}$, dissociation of $G_{\beta\gamma}$, and subsequent opening of glutamate-permeable, two-pore domain potassium channel TREK-1 through direct interaction between $G_{\beta\gamma}$ and N terminus of TREK-1. The slow mode is Ca^{2+} dependent and requires $G_{\alpha q}$ activation and opening of glutamate-permeable, Ca^{2+}-activated anion channel Best1. Ultrastructural analyses demonstrate that TREK-1 is preferentially localized at cell body and processes, whereas Best1 is mostly found in microdomains of astrocytes near synapses. Diffusion modeling predicts that the fast mode can target neuronal mGluR with peak glutamate concentration of 100 μM, whereas slow mode targets neuronal NMDA receptors at around 1 μM. Our results reveal two distinct sources of astrocytic glutamate that can differentially influence neighboring neurons.

INTRODUCTION

Glutamate is the principal excitatory neurotransmitter in the brain. In the central nervous system, both neurons and astrocytes are known to release glutamate; the neuronal glutamate mediates fast synaptic transmission (Traynelis et al., 2010), whereas the astrocytic glutamate appears to modulate synaptic transmission (Haydon and Carmignoto, 2006). Although it is clear that neurons release glutamate via Ca^{2+}-dependent exocytosis, the mechanism of astrocytic glutamate release has been heavily debated, and many controversial issues have been raised (Hamilton and Attwell, 2010; Nedergaard et al., 2002). The field seems to be divided into three conflicting views: (1) astrocytes release glutamate by vesicular exocytosis, just like neurons (Bezzi et al., 2004; Jourdain et al., 2007); (2) Ca^{2+}-dependent astrocytic glutamate does not do anything important (Agulhon et al., 2010); or (3) glutamate is released from astrocytes by transporters or channels (Cavelier and Attwell, 2005; Hamilton and Attwell, 2010; Li et al., 2012; Takano et al., 2005; Ye et al., 2003). Such controversies most likely stem from the inconsistencies in procedures used to increase intracellular Ca^{2+}, such as UV photostimulation (Parpura et al., 1994), mechanical stimulation (Araque et al., 1998, 2000; Montana et al., 2004), electrical stimulation (Jourdain et al., 2007; Kang et al., 1998), uncaging of caged Ca^{2+} or IP_3 (Araque et al., 1998; Fiacco and McCarthy, 2004; Parpura and Haydon, 2000), and G-protein-coupled receptor (GPCR) agonists (Lee et al., 2007; Takano et al., 2005). More importantly, there is no sensitive method to detect glutamate release from individual astrocytes. Conventional techniques include fluorescence imaging of glutamate dehydrogenase activity through NAD^+ to NADH conversion (Innocenti et al., 2000), detection of preloaded radioactive glutamate release (Farinelli and Nicklas, 1992), and high-performance liquid chromatography (HPLC) (Obrenovitch and Zilkha, 2001; Takano et al., 2005). However, these methods lack the desired submillisecond temporal resolution. In contrast, it has been

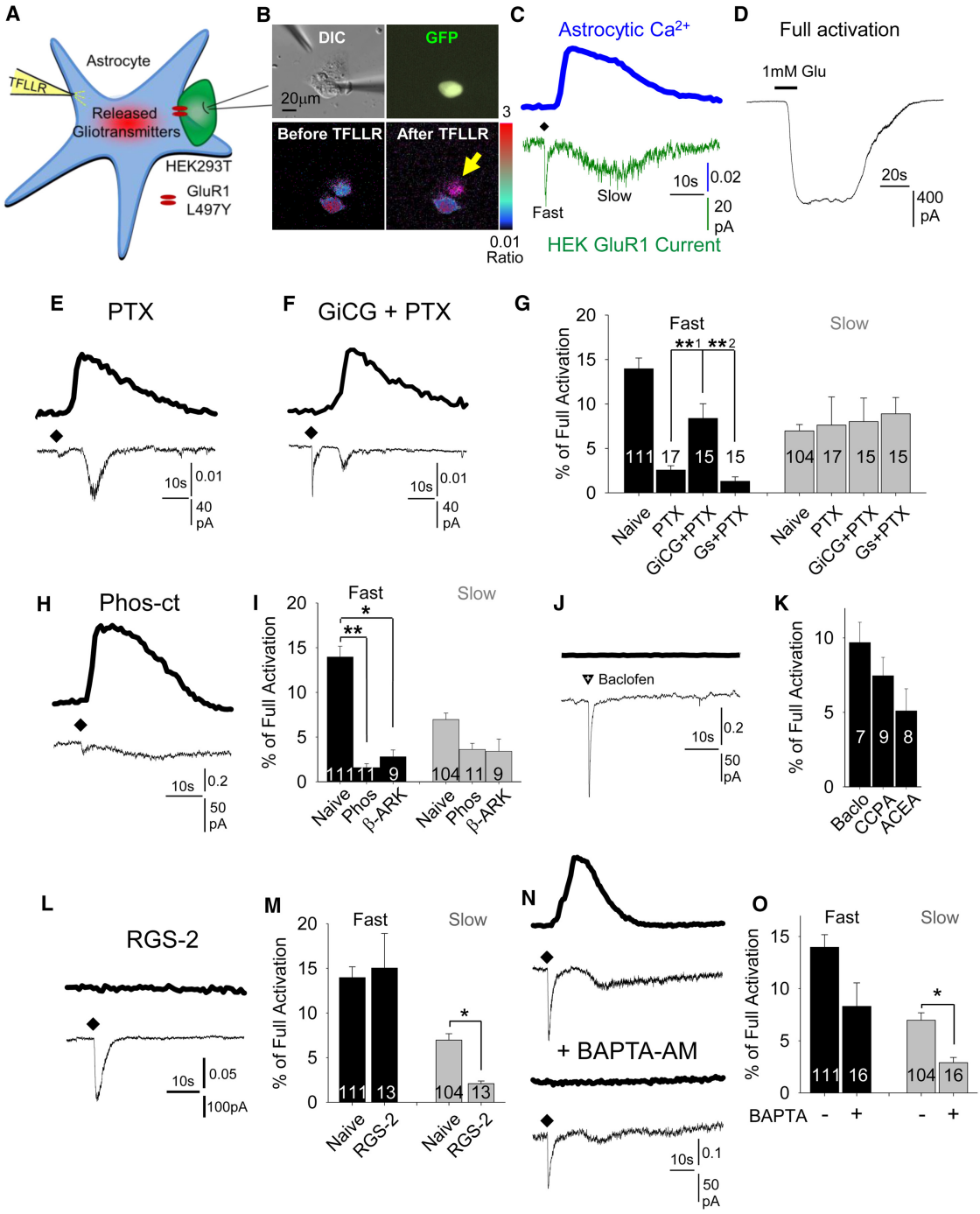

Figure 1. Signaling Pathway of the Receptor-Mediated Glutamate Release from a Single Astrocyte

(A) Schematic illustration for sniffer-patch technique. Left pipette (yellow), pressure application of TFLLR. Right pipette, recording pipette for HEK293T cell expressing GluR1-L497Y (green, sensor cell). Red cloud, gliotransmitters released from cultured astrocyte (blue) upon TFLLR application.

(B) Images for sniffer patch. DIC image (upper left), two cells with two glass pipettes. GFP image (upper right), sensor cell expressing GluR1-L497Y and EGFP. Pseudocolor images, Fura-2 loaded astrocyte (source cell) and sensor cells before TFLLR (lower left) and after TFLLR (lower right). Yellow arrow, increased Ca^{2+} in astrocyte.

(C) Representative traces recorded from sniffer-patch technique. Blue trace, Ca^{2+} transient recorded from astrocyte. Green trace, whole-cell current recorded from sensor cell (V_h = −70mV) upon TFLLR pressure application. Diamond, TFLLR application (10 psi, 100 ms, 500 μM).

(D) Full activation current recorded by bath application of 1 mM glutamate in sensor cell to measure total surface expression of GluR1-L497Y.

(E) Lower current trace, almost complete inhibition of fast mode after treating with 1 μg/ml PTX (12–18 hr).

(F) Lower current trace, a rescue of fast mode in PTX-treated astrocyte overexpressing GiCG.

relatively easy to understand the exocytosis-mediated release of glutamate from presynaptic vesicles because of the availability of high-sensitivity sensors for synaptic glutamate release, namely the postsynaptic AMPA and NMDA receptors (Clements et al., 1992).

In our previous study, we developed the "sniffer-patch" technique, a highly sensitive method for detecting astrocytic glutamate release that is based on a biosensor consisting of HEK293T cells that transiently express a nondesensitizing mutant form of the AMPA receptor subunit, GluR1-L497Y (Lee et al., 2007). This receptor has a high affinity for glutamate (median effective concentration [EC_{50}] = 6.1 μM), allowing detection of submicromolar glutamate levels, a fast activation rate (submillisecond) for detection of rapid release, and a fast deactivation rate (0.7–1.2 ms) for better kinetic separation of different components of glutamate release (Traynelis et al., 2010). To stimulate individual astrocytes with more physiological stimuli, we activated endogenous GPCRs by pressure-applied TFLLR (Hollenberg et al., 1997), a selective peptide agonist of the protease-activated receptor 1 (PAR1). PAR1 is a GPCR that is activated via serine proteases such as thrombin and plasmin by proteolytic cleavage of the N terminus of the receptor, revealing a tethered ligand with a peptide sequence of SFLLRN, which acts as an agonist (Macfarlane et al., 2001). TFLLR mimics the tethered ligand and has been shown to be more selective to PAR1 over PAR2 than the native peptide sequence, SFLLRN (Hollenberg et al., 1997). PAR1 is functionally expressed in most of CA1 hippocampal astrocytes, but not in CA1 pyramidal neurons (Junge et al., 2004), and is linked to $G_{i/o}$, $G_{q/11}$, and G_{12} proteins (Sorensen et al., 2003).

In the present study, we utilized the sniffer patch to dissect the detailed mechanism of GPCR-induced glutamate release in astrocytes. We found that astrocytes release glutamate not by conventional vesicular exocytosis but by the opening of glutamate-permeable ion channels. Furthermore, we found that the drugs or agents that are assumed to inhibit exocytosis and are used to support the vesicular theory of astrocytic glutamate release strongly reduced the surface expression of multiple ion channels, including those that mediate glutamate release.

RESULTS

Characterization of Fast and Slow Modes of Glutamate Release

The general scheme of sniffer patch is illustrated in Figure 1A. On the day of experiment, sensor cells were mixed with astrocytes and allowed to randomly settle on top of individual astrocytes (Figure S1A available online). The sensor cell was then whole-cell patch clamped to monitor released glutamate from its nearby astrocyte. TFLLR was applied while simultaneously monitoring Fura-2 intensity ratio for astrocytic Ca^{2+} signal (Figures 1B and 1C) (Lee et al., 2007).

Upon TFLLR application, glutamate release was detected as an inward current in the sensor cell mediated by GluR1-L497Y. Glutamate release consisted of both fast (latency: 120.0 ± 13.3 ms, n = 33) and slow (time at the peak: 20.2 ± 2.5 s, n = 33) modes (Figure 1C). TFLLR application never induced a current in the sensor cell in the absence of an astrocyte (Figures S1C and S1G). In the presence of astrocyte buffer without TFLLR or RLLFT, a reverse peptide of TFLLR never caused a sensor current (Figures S1D and S1E). However, SFLLR caused a robust sensor current (Figure S1F), just like TFLLR. Bath application of 1 mM glutamate was used to fully activate the GluR1-L497Y channels expressed in the sensor cell (Figure 1D) and to thereby estimate the percent of full activation of GluR1-L497Y activated by astrocytic glutamate release. This percentage can be easily converted to the concentration of glutamate, based on the concentration-response relationship of GluR1-L497Y (Lee et al., 2007). Each response could be categorized into three groups: fast only, slow only, and both modes (Figures S1H–S1J). Most of astrocytes fell into the "both" category (69.3%), though the existence of fast-only (18.1%) and slow-only (12.6%) responses raised the possibility that each component is mediated by a distinct mechanism. The average fraction of receptor activation at the peak of response was greater for the fast mode than for the slow (Figure S1K). However, the total charge was much greater for the slow mode than for the fast (Figure S1L). These two modes and the full-activation current were almost completely blocked by the AMPA receptor blocker CNQX (Figures S1H–S1J, right panels, S1M, and S1B), indicating that glutamate is responsible for both the fast and slow modes. The TFLLR-induced glutamate release was readily repeatable with 10 min intervals (Figure S1N). The fast mode preceded the onset of TFLLR-induced Ca^{2+} increase (Figures 1C and S1O–S1Q), implying the involvement of a Ca^{2+}-independent release mechanism. In contrast, the slow mode occurred in association with the rise of astrocytic Ca^{2+} (Figure S1R), implying a Ca^{2+}-dependent mechanism. The response to the fast mode of astrocytic glutamate release was as fast as the response to exocytosis-mediated neuronal release, suggesting a very rapid mechanism (Figures S1S–S1X).

To examine the signaling pathways mediating the fast and slow modes of glutamate release, we utilized various molecular and pharmacological tools. Because the PAR1 receptor is linked

(G) Summary bar graph for percentage of full activation in each indicated condition (**1, p = 0.005; **2, p = 0.001; unpaired t test). Number on each bar indicates n for each condition.
(H) Lower current trace, inhibition of fast mode in astrocyte overexpressing C terminus of phosducin (Phos-ct).
(I) Summary bar graph for C terminus of phosducin and β-ARK (*p = 0.015; **p = 0.002).
(J) Representative trace for Baclofen (inverted triangle, 100 ms, 300 μM).
(K) Summary graph for percentage of full activation of G_i-coupled GPCR agonists. CCPA (100 ms, 1 μM) and ACEA (100 ms, 300 μM) induce fast mode.
(L) Lower trace, inhibition of slow mode in astrocyte overexpressing RGS-2.
(M) Summary graph for RGS-2-expressing astrocytes (*p = 0.032).
(N) Representative traces for before and after 20 μM BAPTA-AM (30 min) treatment in the same astrocyte/sensor cell.
(O) Summary graph for BAPTA-AM treatment (*p = 0.031).
All values are mean ±SEM. See also Figures S1 and S2.

to both $G_{i/o}$ and $G_{q/12}$, we selectively inhibited the G_i pathway by preincubating astrocytes with pertussis toxin (PTX), which is known to inhibit the action of G_i subunit by ADP-ribosylation (West et al., 1985). We found that PTX selectively and almost completely blocked the fast, but not the slow, mode of glutamate release (Figures 1E and 1G) without affecting astrocytic Ca^{2+} responses (Figures S2A and S2B). This selective inhibition by PTX was significantly rescued by overexpression of a PTX-insensitive form of G_i (Figures 1F and 1G) (Digby et al., 2008), but not by overexpression of the G_s subunit (Figure 1G). Activation of GPCRs is known to dissociate the $G_{\beta\gamma}$ complex from the trimeric G_i-$G_{\beta\gamma}$ complex (Koch et al., 1993). Thus, we further tested the role of G_i by asking whether disturbing the $G_{\beta\gamma}$ dissociation affects the fast mode. Overexpression of the C terminus of phosducin or β-ARK, which has been reported to inhibit $G_{\beta\gamma}$ dissociation (Blüml et al., 1997; Koch et al., 1993), almost completely inhibited the fast mode (Figures 1H and 1I) without affecting the Ca^{2+} responses (Figures S2C and S2D). Furthermore, well-known agonists of G_i-coupled GPCR could induce fast glutamate release; baclofen, $GABA_B$ agonist, 2-chloro-N(6)-cyclopentyladenosine (CCPA), adenosine receptor A1 agonist, arachidonyl-2′-chloroethylamide (ACEA), and cannabinoid receptor CB1 agonist all activated a fast mode of glutamate release, which was similar to that induced by TFLLR, without a measurable Ca^{2+} increase or a slow mode of glutamate release (Figures 1J, 1K, S2G, and S2H).

To examine the involvement of G_q signaling, we overexpressed RGS-2, which is reported to selectively inhibit the G_q subunit (Heximer et al., 1997). We found that RGS-2 overexpression selectively and significantly inhibited both the slow mode of glutamate release and the associated Ca^{2+} increase while not affecting the fast mode (Figures 1L, 1M, S2E, and S2F). G_q signaling activates phospholipase Cβ, producing IP_3 and releasing Ca^{2+} through the IP_3R channel (Clapham, 2007). Thus, we tested the sensitivity of slow mode to the Ca^{2+} chelator, BAPTA. We found that 30 min treatment with BAPTA-AM eliminated the TFLLR-induced Ca^{2+} response and significantly reduced the slow mode, but not the fast mode (Figures 1N and 1O). These results indicate that the slow mode is preferentially linked to G_q signaling and subsequent Ca^{2+} release. To test the involvement of G_s, which produces cyclic AMP (cAMP), we applied TFLLR in the presence of IBMX, an inhibitor of cAMP phosphodiesterase, or forskolin, an activator of adenylyl cyclase, and found no evidence for the involvement of cAMP in the fast or slow components of glutamate release (Figures S2I–S2K).

Vesicular Exocytosis Is Not Involved

Next, we examined whether vesicular exocytosis is involved in the fast and slow modes of glutamate release. First, we applied hyperosmotic solution, which causes exocytotic release of glutamate in neurons (Bekkers and Stevens, 1995), and found that this evoked no glutamate release from astrocytes (Figures S3A and S3C; Lee et al., 2007). Unlike neurons, astrocytes apparently do not possess glutamate-containing vesicles sensitive to hyperosmotic solution. Rose Bengal, which inhibited glutamate released by mechanical stimulation (Montana et al., 2004), did not have any effect on the fast or slow modes of glutamate released by TFLLR (Figures S3B and S3C). Treatment of astrocytes with Bafilomycin A1 and Concanamycin A, which should deplete glutamate from synaptic vesicles, appeared to block both fast and slow modes, presumably due to the fact that these compounds almost completely eliminated the surface expression of GluR1-L497Y in the sensor cell (Figures S3D–S3G, S3I, and S3K). Tetanus toxin (TeTX) also caused the similar effect of removing surface GluR1-L497Y (Figures S3J and S3K), complicating the interpretation of any results obtained using this toxin. To avoid the effects of drugs and toxins on the sensor cell, we injected Botulinum toxin B (BoToxB), together with Ca^{2+} indicator dye Fura-2, into individual astrocytes through the patch pipette. This did not cause any significant effect on the surface expression of GluR1-L497Y on the sensor cell (Figures S3M and S3P). We found that BoToxB injection did not have any effect on TFLLR-induced fast and slow modes (Figures 2A and 2C), although it completely eliminated glutamate release in the same astrocyte in response to mechanical stimulation (Figures 2A and 2D), as previously reported (Araque et al., 2000). In contrast, TeTX injection substantially decreased the surface expression of GluR1-L497Y in the sensor cell within 20 min (Figures S3L and S3P) and TFLLR-induced glutamate release (Figures S3L and S3O), suggesting that TeTX can readily cross the astrocytic membrane and affect the surface expression of GluR1-L497Y in the neighboring sensor cell. As a control experiment, we injected bovine serum albumin (BSA), instead of BotoxB, and found that BSA did not have any effect on TFLLR-induced fast and slow modes of glutamate release (Figures 2B, 2C, S3N, and S3O) or on mechanical stimulation-induced glutamate release, as expected (Figures 2B and 2D). From these results, we conclude that, whereas the glutamate released by mechanical stimulation is sensitive to inhibitors of exocytosis, glutamate released by TFLLR is not.

Molecular Identities of Fast and Slow Modes of Glutamate Release

We next examined the possibility that TFLLR induces glutamate release from astrocytes via channels or transporters. We screened blockers of various channels and glutamate transporters and found that both the fast and slow modes of release were blocked by blockers of Ca^{2+}-activated anion channel (CAAC), such as NPPB, niflumic acid, DIDS (Figures 2E, S4A, and S4B), and quinine, which blocks two-pore potassium (K2P) channels (Figures 2F and S4C). Although these blockers are notorious for their nonspecific effects (Greenwood and Leblanc, 2007; Wang et al., 1997), they did not have any effect on the sensor, GluR1-L497Y (Figures S4D and S4E). Blockers that did not show any significant effect include TTX (voltage-gated sodium channels), Cd^{2+} (voltage-gated Ca^{2+} channels), TEA, Ba^{2+}, Cs^+ (potassium channel), CBX (gap junction hemichannel), and DCPIB (volume-sensitive anion channel) (Figure S4G). PPADS (P2X channel) appeared to block the fast mode (Figure S4G), but this was not interpretable because PPADS had nonspecific effects (Figures S4E and S4H–J). From the results of this screening, CAAC and K2P channels emerged as strong candidates as molecular mediators of receptor-mediated glutamate release from astrocytes.

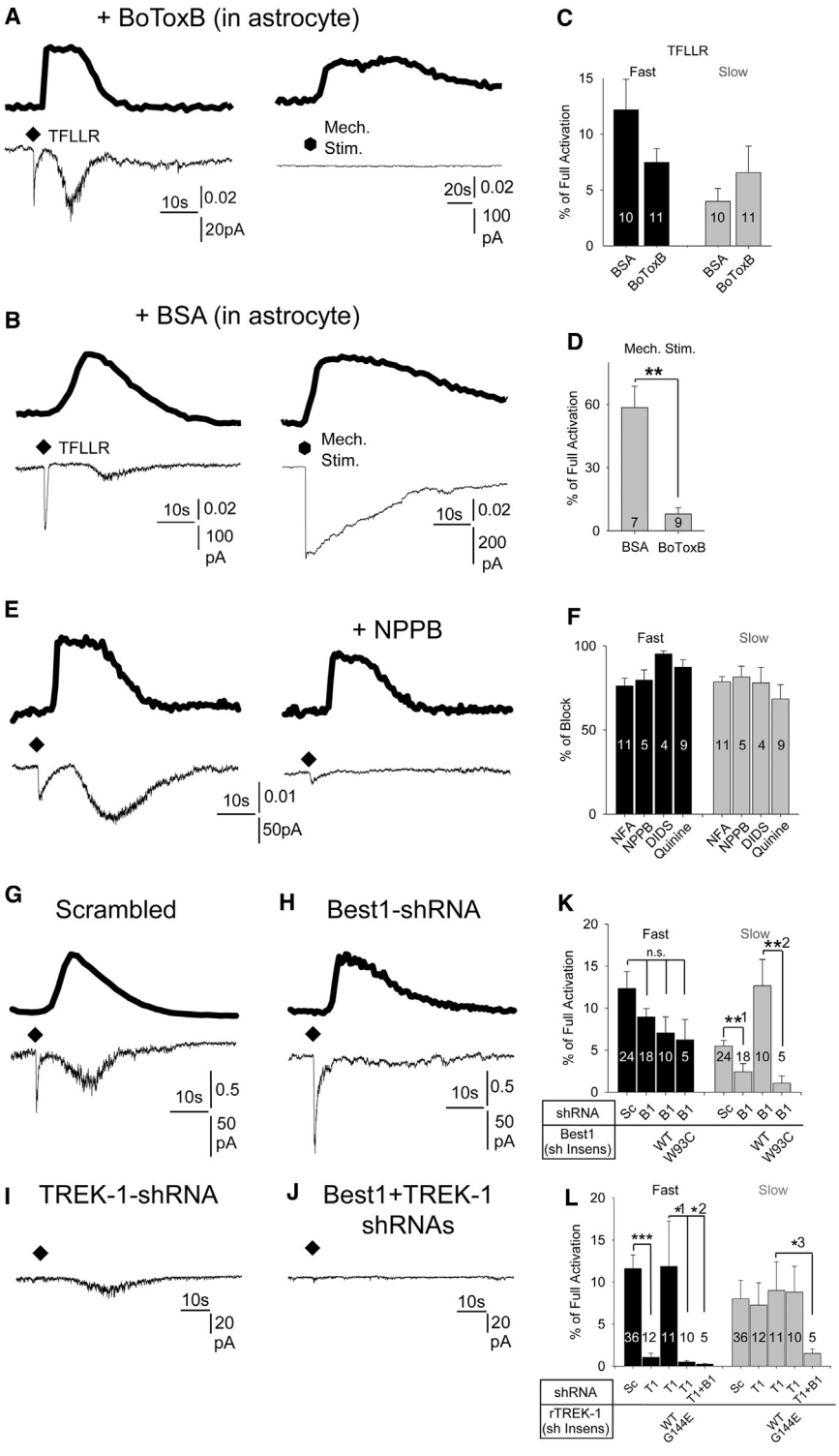

Figure 2. Molecular Identities of Fast and Slow Glutamate Release

(A) Traces for BoToxB-injected astrocyte (8 μg/ml, 20 min) stimulated with TFLLR (left) and mechanical stimulation (right). Diamond, TFLLR application (100 ms, 500 μM). Hexagon, mechanical stimulation.

(B) Traces for BSA-injected astrocyte (8 μg/ml, 20 min).

(C) Summary graph for BotoxB and BSA injection.

(D) Summary graph for mechanical stimulation (*p = 0.001).

(E) Traces for glutamate release before (left) and during 50 μM NPPB (right).

(F) Summary graph for percentage of block by DIDS (50 μM for 10 min), DCPIB (50 μM for 10 min), and quinine (100 μM for 10 min).

(G–J) Traces for each astrocyte overexpressing control scrambled shRNA (G), Best1-shRNA (H), TREK-1-shRNA (I), and both Best1- and TREK-1-shRNAs (J).

(K) Summary graph for astrocytes overexpressing Best1-shRNA and coexpressing Best1-shRNA-insensitive, wild-type, and W93C pore mutant form of Best1 cDNA (**1, p = 0.008; **2, p = 0.009; n.s., nonsignificance).

(L) Summary graph for astrocytes overexpressing TREK-1-shRNA and coexpressing rat TREK-1 cDNA, wild-type, and G144E, insensitive for TREK-1-shRNA (***p = 0.0004; *1, p = 0.047; *2, p = 0.012; *3, p = 0.048).

All values are mean ±SEM. See also Figures S3, S4, and S7.

To determine the molecular identity of the slow mode, we first tested the Bestrophin-1(Best1) channel because this Ca^{2+}-activated anion channel is highly expressed in hippocampal astrocytes (Park et al., 2009). It also shows unique properties such as permeability to glutamate (Park et al., 2009) and GABA (Lee et al., 2010). Although Best1 channel is permeable to both glutamate and GABA, it is not likely to mediate GABA release from hippocampal astrocytes because hippocampal astrocytes do not contain GABA (Yoon et al., 2011), unlike the cerebellar Bergmann glial cells (Lee et al., 2010). Silencing the Best1 gene via specific small hairpin RNA (shRNA) for mouse Best1 selectively reduced the slow mode without significantly affecting the fast mode (Figures 2G, 2H, and 2K). This effect was specific because it was not observed with a control scrambled shRNA and was fully rescued by the cotransfection of Best1-shRNA, along with an shRNA-insensitive form of Best1 (Figure 2K). However, the addition of a pore mutation at position 93, from tryptophan to cysteine (Best1-W93C) (Zhang et al., 2010), failed to rescue the slow mode, indicating that permeation of glutamate through the pore of Best1channel is responsible for the slow mode (Figure 2K).

For the fast mode, we next explored the possibility of TREK-1, which is a recently proposed K2P channel in astrocytes (Zhou et al., 2009). An shRNA specific for mouse TREK-1 was

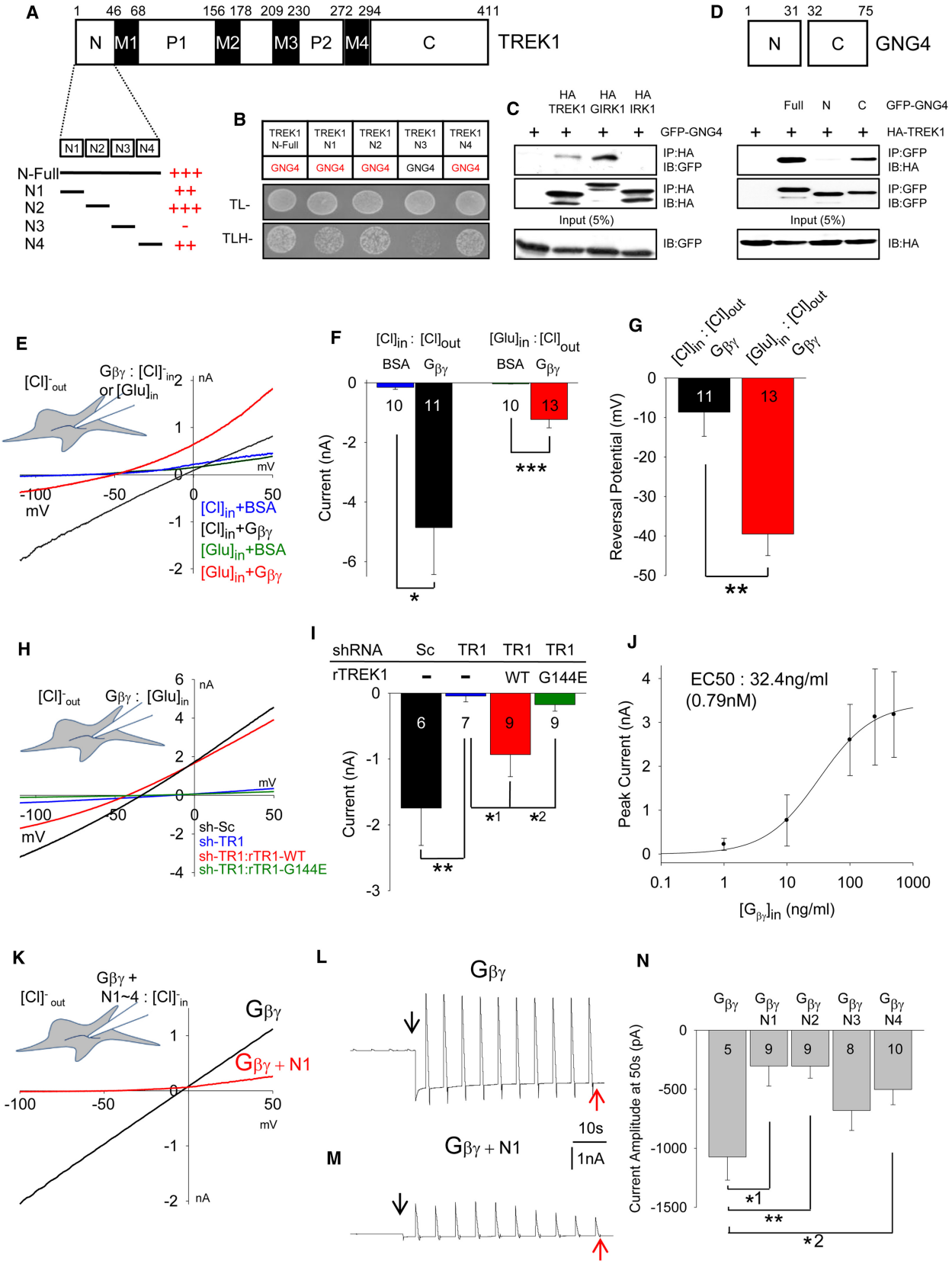
A
1 46 68 156 178 209 230 272 294 411
N M1 P1 M2 M3 P2 M4 C
TREK1
N1 N2 N3 N4
N-Full +++
N1 ++
N2 +++
N3 -
N4 ++
B
TREK1 N-Full
TREK1 N1
TREK1 N2
TREK1 N3
TREK1 N4
GNG4
TL-
TLH-
C
HA TREK1
HA GIRK1
HA IRK1
GFP-GNG4
IP:HA IB:GFP
IP:HA IB:HA
Input (5%)
IB:GFP
Full N C GFP-GNG4
HA-TREK1
IP:GFP IB:HA
IP:GFP IB:GFP
Input (5%)
IB:HA
D
1 31 32 75
N C GNG4
E
[Cl]-out
Gβγ : [Cl]-in or [Glu]in
nA
mV
-100 mV
-50
50
[Cl]in+BSA
[Cl]in+Gβγ
[Glu]in+BSA
[Glu]in+Gβγ
F
[Cl]in : [Cl]out
[Glu]in : [Cl]out
BSA Gβγ
Current (nA)
10 11 10 13
***
*
G
[Cl]in : [Cl]out Gβγ
[Glu]in : [Cl]out Gβγ
Reversal Potential (mV)
11 13
**
H
[Cl]-out
Gβγ : [Glu]in
nA
mV
-100 mV
-50
50
sh-Sc
sh-TR1
sh-TR1:rTR1-WT
sh-TR1:rTR1-G144E
I
shRNA Sc TR1 TR1 TR1
rTREK1 - - WT G144E
Current (nA)
6 7 9 9
**
*1
*2
J
EC50 : 32.4ng/ml
(0.79nM)
Peak Current (nA)
0.1 1 10 100 1000
[Gβγ]in (ng/ml)
K
[Cl]-out
Gβγ + N1~4 : [Cl]-in
Gβγ
Gβγ + N1
-100 -50 50 mV
nA
L
Gβγ
10s
1nA
M
Gβγ + N1
N
Gβγ Gβγ N1 Gβγ N2 Gβγ N3 Gβγ N4
Current Amplitude at 50s (pA)
5 9 9 8 10
*1
**
*2

developed (Figures S4K–M) and tested for effects on glutamate release. Gene silencing of TREK-1 selectively eliminated the fast mode without affecting the slow mode (Figures 2I and 2L) and was fully rescued by rat TREK-1, which is insensitive to mouse TREK-1-shRNA (Figure 2L). However, the addition of a pore mutation at position 144, from glycine to glutamate (rTREK-1-G144E) (Brenner and O'Shaughnessy, 2008), failed to rescue the fast mode. Finally, cotransfecting the shRNAs for Best1 and TREK-1 eliminated both the fast and slow modes (Figures 2J and 2L).

Opening of Glutamate-Permeable Channel by Direct Binding of $G_{\beta\gamma}$ to TREK-1

How can TREK-1, a potassium channel, conduct and release glutamate? TREK-1-mediated glutamate release is relatively fast and requires G_i-$G_{\beta\gamma}$ dissociation. To answer the question, we considered a possibility that $G_{\beta\gamma}$ directly binds to TREK-1 to open a glutamate-permeable channel. A previous yeast two-hybrid screen suggested that N terminus of TREK-1 interacts with GNG4 (subtype 4 of G_γ subunit) (Kim et al., 2010). Therefore, we performed a detailed analysis of N-terminal region of TREK-1 by yeast two-hybrid assay (Figures 3A and S5A). Of the four segments of N-terminal region of TREK-1, each with 11 or 12 amino acid residues, we found that the N1, N2, and N4 segments strongly interacted with GNG4, whereas N3 did not (Figures 3A, 3B, and S5B). The interaction of TREK-1 N terminus with GNG4 was also confirmed by MBP pull-down assay (Figure S5C). We confirmed the interaction between full-length TREK-1 and GNG4 via coimmunoprecipitation by using the antibodies against hemagglutinin (HA) and green fluorescent protein (GFP) after heterologously expressing GFP-GNG4 and HA-TREK-1 in HEK293T cells (Figure 3C). As a positive and negative control, we performed similar experiments with a well-known $G_{\beta\gamma}$-interacting channel, GIRK (G-protein-coupled inwardly rectifying potassium channel), and a noninteracting IRK (inwardly rectifying potassium channel). We found that GIRK strongly interacted with GNG4, whereas IRK did not (Figure 3C), as expected (Huang et al., 1995). Furthermore, RT-PCR analysis showed that cultured astrocytes express GNG4 (Figure S5G).

To map out the region of GNG4 that interacts with TREK-1, we divided the GNG4 protein sequence (75 amino acids) into two segments, N (1–31)- and C (32–75)-terminal segments, and checked for protein-protein interaction with full-length TREK-1 by coimmunoprecipitation (Figure 3D). The results showed that C terminus of GNG4 showed strong interaction with TREK-1, whereas N terminus did not (Figure 3D). To test the specificity of different GNG isoforms, we first cloned 11 out of 12 known isoforms of GNG family from the complementary DNAs (cDNAs) of primary cultured mouse astrocytes. The analysis of sequence homology between isoforms indicated that there are well-conserved N-helix and C-helix (Figure S5H), and the phylogenic tree indicated a close homology between GNG1 and GNG11 and between GNG5 and GNG10 (Figure S5I and Table S1). Then we performed a coimmunoprecipitation experiment for each GNG isoform against TREK-1 and found that most GNG isoforms coimmunoprecipitated with TREK-1 protein. In contrast, GNG5 and GNG10 showed a lack of interaction, and GNG1 and GNG11 showed a weak interaction (Figure S5J), indicating that GNG binding to TREK1 is isoform specific.

We then asked whether $G_{\beta\gamma}$ can directly open any channels in cultured astrocytes. We performed whole-cell current recording with purified $G_{\beta\gamma}$ in the patch pipette and found that a large inward current was induced by intracellularly applied $G_{\beta\gamma}$ upon the membrane rupture ($V_h = -70$mV). Surprisingly, the reversal potential of this current (-3.8 ± 0.2mV, n = 19) was far away from the equilibrium potential for K^+ (-70mV) or Na^+ (40mV) but was near the Cl^- equilibrium potential (0mV; Figures S5D–S5F). Ion substitution experiments showed that the $G_{\beta\gamma}$-induced current was mostly carried by Cl^- ion because of the linear current-voltage (I-V) relationship and reversal potential near 0mV, which was observed when identical Cl^- concentrations were present on both sides of the plasma membrane (Figure 3E, black trace). As a control, we used BSA, which did not induce any significant current (Figure 3E, blue trace). To determine whether the conductance shows permeability to glutamate, we substituted Cl^- in the intracellular pipette solution with glutamate and found that $G_{\beta\gamma}$ induced a significant inward current at -100mV with reversal potential around -40mV (Figure 3E,

Figure 3. Direct Interaction between $G_{\beta\gamma}$ and TREK-1 Induces Anion Conductance in Astrocyte

(A) A schematic illustration represents various domains and amino acid (aa) sequence of TREK-1. M1-4, four transmembrane domains. P1 and P2, pore domains. The N terminus (1–46 aa) is divided into four segments, N1–4. Red pluses, degree of interaction between indicated region of TREK-1 and GNG4 from Y2H.

(B) Interaction between subdomains (N1–4) of TREK-1 and GNG4 by the presence of yeast colony in TLH− (tryptophan, leucine, and histidine).

(C) Co-IP assays showing that TREK-1, as well as GIRK1, interacts with GNG4, but not with IRK1.

(D) GNG4 domain (top). Co-IP assays showing that C terminus of GNG4 interacts with TREK-1, but not N terminus (bottom).

(E) I-V curves for $G_{\beta\gamma}$-induced conductance with chloride (black) or glutamate (red) and BSA-induced conductance with chloride (blue) or glutamate (green). Inset, schematic diagram for experiment (in mM, 150 $[Cl]_{in}$, 150 $[Glu]_{in}$, 6.09 nM $G_{\beta\gamma}$: 150 $[Cl]_{out}$).

(F) Summary graph for four conditions with different internal solutions (*p = 0.019; ***p = 0.0004).

(G) Summary graph for reversal potential (**p = 0.001).

(H) I-V curves show that glutamate permeability depends on TREK-1. Inset, 150 mM $[Glu]_{in}$, 6.09 nM $G_{\beta\gamma}$: 150 mM $[Cl^-]_{out}$. $G_{\beta\gamma}$-induced conductance with TREK-1 shRNA (blue). Coexpression of rat TREK-1 and TREK-1 shRNA (red). G144E of rat TREK-1 and TREK-1 shRNA (green).

(I) Summary bar graph for current amplitude at -100mV (**p = 0.008; *1, p = 0.038; *2, p = 0.045).

(J) Concentration-response relationship for $G_{\beta\gamma}$ on the conductance under chloride condition (mM, 150 $[Cl^-]_{in}$: 150 $[Cl^-]_{out}$).

(K) I-V curves show that chloride conductance depends on the competitive peptide. $G_{\beta\gamma}$-induced conductance (black) with N1 peptide (red). Inset, 150 mM $[Cl^-]_{in}$, 6.09 nM $G_{\beta\gamma}$: 150 mM $[Cl^-]_{out}$.

(L and M) Traces for $G_{\beta\gamma}$-induced current upon membrane rupture (black arrow) (L) and with 100 μM N1 peptide (M). Red arrows, point of current amplitude is measured (50 s).

(N) Summary bar graph.

All values are mean ±SEM. (*1, p = 0.015; **p = 0.002; *2, p = 0.026.) See also Figure S5.

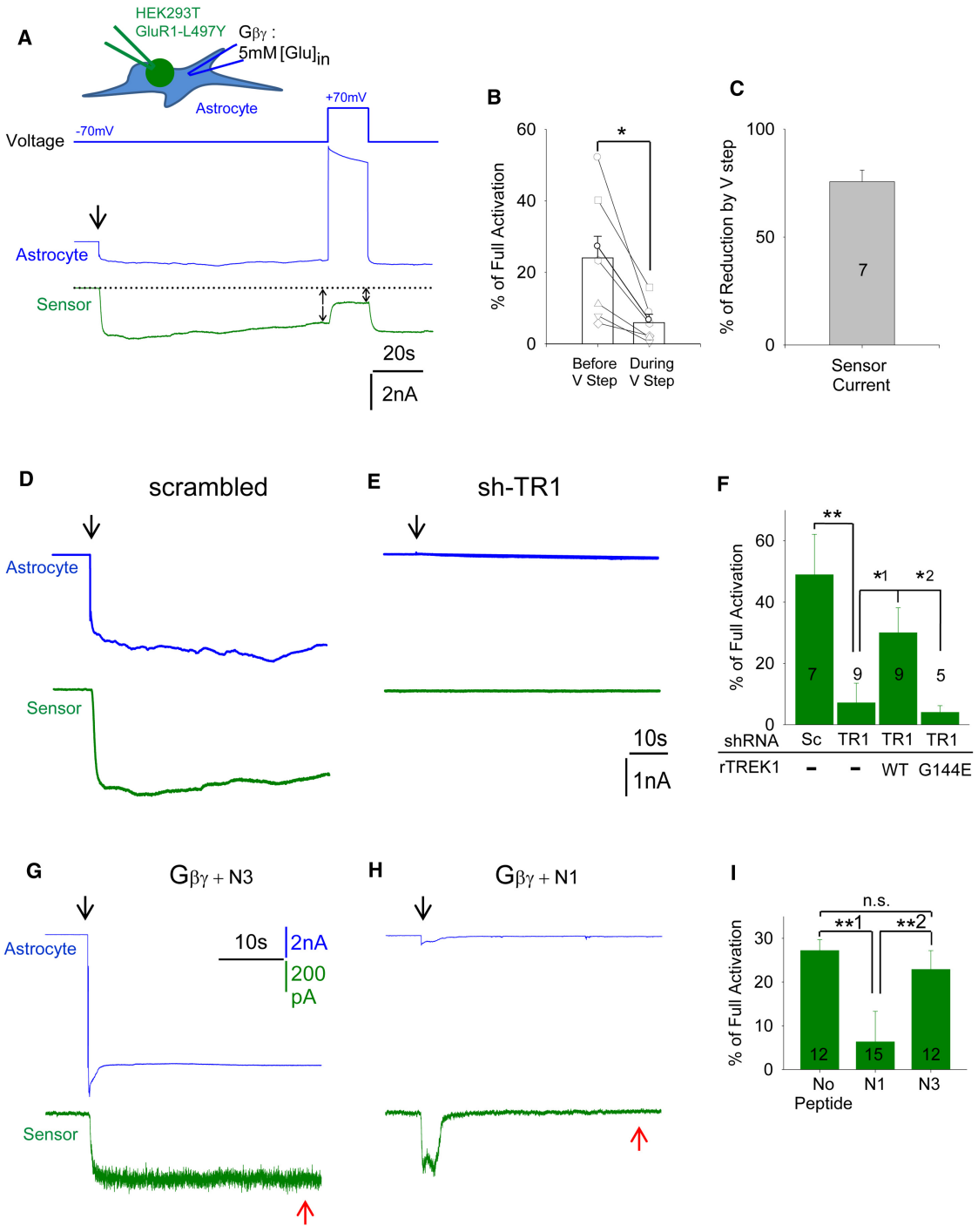

Figure 4. Direct Binding of $G_{\beta\gamma}$ Protein to TREK-1 Causes Release of Glutamate

(A) A schematic diagram for two-cell sniffer patch. Green cell, HEK293T cell expressing GluR1-L497Y. Blue cell, astrocyte. Blue lines, glass pipette containing 5 mM glutamate and 6.09 nM $G_{\beta\gamma}$. Green lines, glass pipette for patching sensor cell. First blue trace, change of holding voltage (Vh) on astrocyte from −70mV to 70mV. Current traces both from astrocyte (middle blue) and sensor cell (green). Arrow, point of membrane rupture. Upon voltage step Vh = +70mV in astrocyte (middle blue), the current amplitude of sensor current (green) decreased. Dotted line, baseline current level. Arrows, measurement of sensor currents.

(B) Summary bar graph for indicated conditions (*p = 0.032, paired t test).

(C) Summary bar graph for percentage of current reduction in response to voltage step.

(D) Two-cell sniffer-patch assay. Blue trace, astrocyte expressing control scrambled shRNA. Green trace, sensor cell. Arrow, time of membrane rupture on astrocyte.

(E) TREK-1-shRNA-expressing astrocyte and sensor current.

red trace), indicating a significant glutamate permeability. From the average shift in reversal potential of −30.9mV produced by the substitution of intracellular Cl^- with glutamate (Figure 3G), we calculated the permeability ratio of glutamate to Cl^- ($P_{glutamate}/P_{Cl^-}$) to be 0.27 by using the Goldman-Hodgkin-Katz equation. In the absence of $G_{\beta\gamma}$, the conductance for glutamate, as well as that for Cl^-, was negligible (Figure 3F). From the concentration-response relationship, EC_{50} for $G_{\beta\gamma}$ was determined to be 32.4 ng/ml (0.79 nM) (Figure 3J).

To test whether the $G_{\beta\gamma}$-induced glutamate conductance is mediated by TREK-1, we performed a similar experiment after silencing the TREK-1 gene with shRNA. Compared to the scrambled shRNA (Figure 3H black trace and 3I), we found that mouse TREK-1-shRNA eliminated the $G_{\beta\gamma}$-induced conductance (blue trace), which was significantly rescued by coexpression of rat TREK-1 (red trace). The pore mutant rTREK-1-G144E failed to rescue the $G_{\beta\gamma}$-induced conductance (green trace). These results indicate that TREK-1 mediates the glutamate conductance induced by $G_{\beta\gamma}$. Because N1, N2, and N4 of TREK-1 interact with GNG4, we tested for functional interaction by using these competitive peptides. Inclusion of competitive peptides N1, N2, and N4 in the patch pipette significantly reduced $G_{\beta\gamma}$-induced chloride currents (Figures 3K–3N).

To determine whether activation of TREK-1 by $G_{\beta\gamma}$ can release glutamate from astrocytes, we performed two-cell sniffer patch (Lee et al., 2010). Under this configuration, two patch pipettes were used: one containing both $G_{\beta\gamma}$ and 5 mM glutamate to record from an astrocyte and the other for a sensor cell expressing GluR1-L497Y to detect released glutamate. Upon membrane rupture, the astrocyte showed a large inward current (Vh = −70mV), and the sensor cell displayed a substantial parallel current representing glutamate released from the neighboring astrocyte (Figures 4A and 4B). Outflow of glutamate from astrocyte was dependent on the electrochemical gradient because changing the holding potential from −70mV to +70mV reduced glutamate release by ~75% (Figures 4A–4C), as predicted by the Nernst equation. This glutamate release was eliminated by silencing the TREK-1 gene in astrocytes and was rescued by coexpression of rat TREK-1 (Figures 4D–4F). The pore mutant rTREK-1-G144E failed to rescue (Figure 4F). These results indicate that astrocytic glutamate release can be directly induced by $G_{\beta\gamma}$ and that TREK-1 mediates this release by direct permeation of glutamate through its pore. Finally, we tested whether TREK-1-mediated glutamate release requires direct binding of $G_{\beta\gamma}$ to TREK-1 by utilizing the N-terminal segments of TREK-1 to compete for binding of $G_{\beta\gamma}$ to TREK-1. We performed two-cell sniffer patch and found that N1 peptide significantly reduced the $G_{\beta\gamma}$-induced glutamate release, as well as $G_{\beta\gamma}$-induced current (Figures 4H and 4I), whereas N3 had no significant effect compared to the control condition without any peptide (Figures 4G and 4I).

Best1 Is a Glutamate-Permeable Channel

We recently demonstrated that Best1 channel is activated by intracellular Ca^{2+} (EC_{50} = 150 nM) with considerable permeability to GABA (Lee et al., 2010; Park et al., 2009) and that hippocampal astrocytes express CAAC with glutamate permeability (Lee et al., 2010; Park et al., 2009). To test whether heterologously expressed Best1 is also permeable to glutamate, we measured Best1-mediated anion conductance in HEK293T cells expressing mouse Best1 gene by using patch pipette solution with high Ca^{2+} (4.5 μM free Ca^{2+}) for maximal channel activation and Cl^- or glutamate as the solely permeant anion (145 mM Cl^- or glutamate). The I-V relationship of currents flowing through Best1 was determined as illustrated in Figure 5A (black trace). We found a significant Ca^{2+}-induced conductance carried by the efflux of Cl^- or glutamate at −70mV, which was eliminated by the absence of free Ca^{2+} in the pipette solution (Figures 5A and 5B). The estimated permeability ratio of glutamate and Cl^- was $P_{glutamate}/P_{Cl}$ = 0.67 (E_{rev} of internal Cl^-: 1.9 ± 0.8mV, n = 9; E_{rev} of internal glutamate: −6.4 ± 2.0mV, n = 11; p = 0.0019) according to the Goldman-Hodgkin-Kats equation. These results indicate that Best1 channels show substantial permeability to glutamate, which is consistent with the previous reports (Lee et al., 2010; O'Driscoll et al., 2009; Park et al., 2009).

To determine whether such glutamate efflux through Best1 channel can be detected by a neighboring cell, we performed the two-cell sniffer patch between source cell and sensor cell (Figure 5C; Lee et al., 2010). The internal solution for cells expressing Best1 channel contained Cl^- or glutamate for anion, and upon rupture of membrane, Best1 was activated by high Ca^{2+} in the pipette solution (~4.5 μM free Ca^{2+}; Figure 5C). We found that Best1 displayed a significant glutamate conductance (Figure 5E, top blue trace) and that this current was associated with a sensor current (Figure 5E, bottom green trace). We found that the release of glutamate depended on permeation through Ca^{2+}-activated Best1 (Figure 5D) because it was absent (1) when Best1 was not expressed, (2) when glutamate was replaced by Cl^-, (3) when Ca^{2+} was absent (Figure 5F), and (4) when the source cell expressed the pore mutant of Best1 (W93C).

Differential Localization and Neuronal Targets of TREK-1 and Best1

To see whether the same kind of glutamate release is observed ex vivo, we performed sniffer-patch experiment and recorded CNQX-sensitive glutamate release from a single, acutely isolated, GFP-positive hippocampal astrocyte, which was prepared from the brain slices of adult GFAP-GFP transgenic mice (Figure 6A). We similarly observed fast and slow modes of glutamate release (Figures 6B and 6C) with similar kinetic properties (fast mode latency: 61.5 ± 5.4 ms, n = 15; slow mode peak: 22.5 ± 4.3 s, n = 16). To test whether the same molecules are involved

(F) Summary bar graph for sensor current (green) (**p = 0.008; *1, p = 0.041; *2, p = 0.038).
(G) Current traces for astrocyte injected with $G_{\beta\gamma}$ and N3 peptide (blue) and sensor current (green).
(H) Current trace for astrocyte injected with $G_{\beta\gamma}$ and N1 peptide (blue) and sensor current (green). Black arrow, membrane rupture. Red arrow, measurement point.
(I) Summary bar graph for percentage of full activation (**1, p = 0.005; **2, p = 0.001; n.s., nonsignificance).
All values are expressed as mean ±SEM.

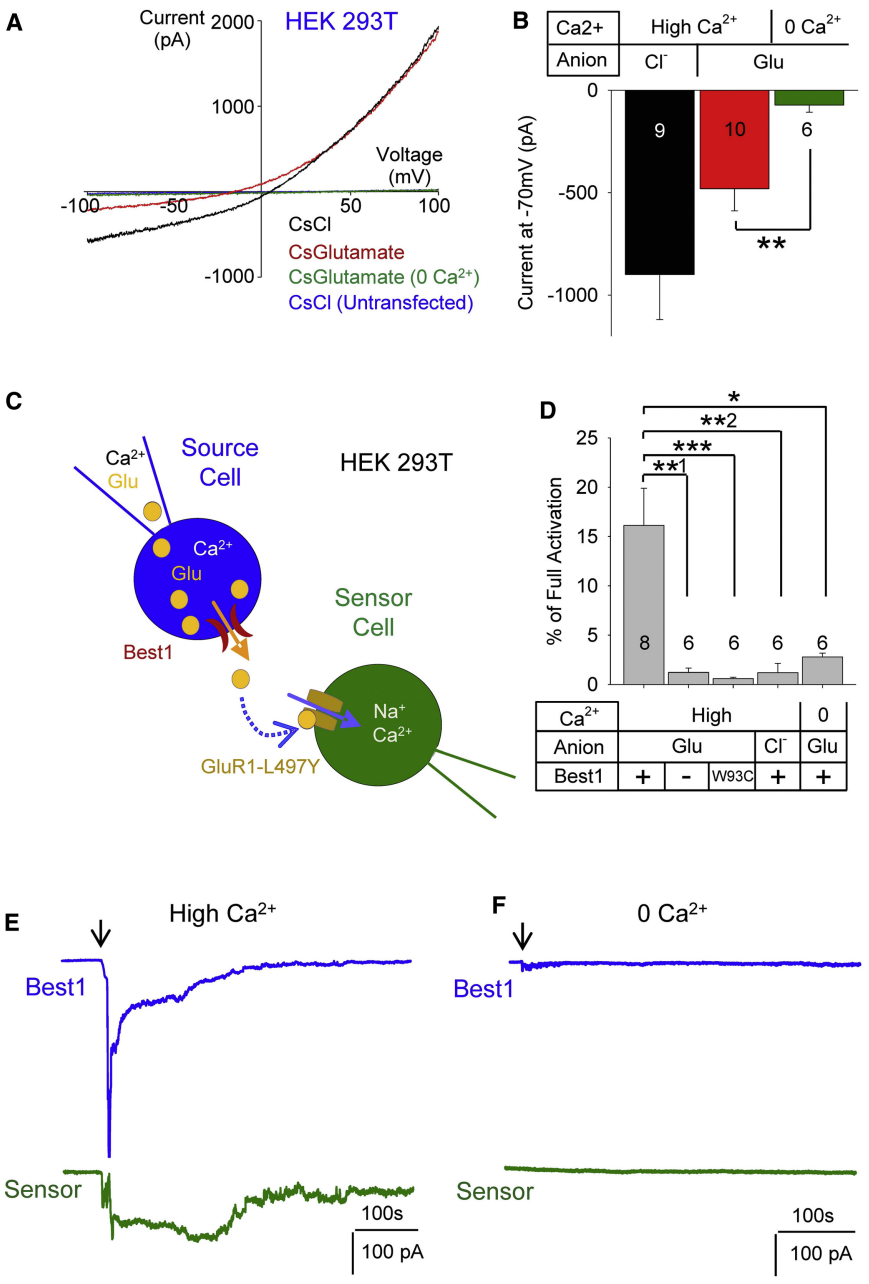

Figure 5. Best1 Releases Glutamate by Ca^{2+}

(A) I-V for HEK293T cells expressing mouse Best1. Pipette solution containing 4.5 μM Ca^{2+} + 145mM Cl^- (Cs-Cl, black trace), 4.5 μM of Ca^{2+} + 145 mM of glutamate (Cs-glutamate, red trace), or 0 μM Ca^{2+} + 145 mM glutamate (Cs-glutamate [0 Ca^{2+}], green trace). Untransfected HEK293T cells using pipette solution containing 4.5 μM of Ca^{2+} + 145 mM Cl^- (untransfected, blue trace).

(B) Summary bar graph for averaged current amplitude at −70mV (*p = 0.03) for each group. Number of cells from at least two independent culture batches is indicated on each bar.

(C) Two-cell sniffer patch using Best1- (source cell) and GluR1L497Y-expressing (sensor cell) HEK293T cells.

(D) Summary bar graph representing averaged responses in sensor cell. The source cells such as wild-type Best1-expressing cells, untransfected cells or Best1W93C (pore mutant)-expressing cells with 4.5 μM Ca^{2+} + 145 mM glutamate-containing pipette solution, Best1-expressing cells with 0 μM Ca^{2+} + 145 mM glutamate-containing pipette solution, and Best1-expressing cells with 4.5 μM Ca^{2+} + 145 mM chloride-containing pipette solution (**1, p = 0.005; ***p = 0.004; **2, p = 0.005; *p = 0.011).

(E and F) Traces for two-cell sniffer patch from Best1-expressing source cell (Best1, blue) and sensor cell (green). Best1-expressing cells were patched and ruptured by using 145 mM glutamate-containing pipette solution with high 4.5 μM Ca^{2+} (E) or 0 μM Ca^{2+} (F). Arrowheads, time point of membrane rupture of source cell.

All average values are expressed as mean ±SEM.

in vivo, we first generated a lentivirus carrying TREK-1 shRNA and injected into wild-type hippocampal CA1 to perform sniffer-patch experiment from acutely isolated astrocytes. We found that TREK-1 shRNA selectively eliminated fast mode, as compared to the scrambled shRNA (Figures 6D and 6G). Then we tested Best1 knockout mice (Figures S7A and S7B; Marmorstein et al., 2006) and found that slow mode was selectively eliminated, as compared to the astrocytes of wild-type mice (Figures 6E and 6G). Finally, TREK-1 shRNA in Best1 knockout mice eliminated both fast and slow modes (Figures 6F and 6G).

Astrocytes show elaborate structures in vivo with several key cellular compartments. Of these structures, microdomains tightly wrap around each synapse (Grosche et al., 1999; Halassa et al., 2007). To determine the subcellular distribution of the Best1 and TREK-1 channels and thus to predict the in vivo function, we performed electron microscopic immunohistochemistry with antisera against Best1 or TREK-1 and against GFP in GFAP-GFP mice. We found that Best1 channels were preferentially expressed at the surface membrane of microdomains adjacent to glutamatergic synapses (Figure 6H), as compared to other cellular compartments such as cell body and large processes (Figures 6J and S6A–S6C). The labeling in the large processes was located inside the processes rather than near or at the plasma membrane (Figure S6B), suggesting that these proteins are being transported out to the distal microdomains. In contrast to Best1, TREK-1 antibody showed opposite distribution pattern—namely, at the surface of cell body and processes, but not at the microdomains (Figures 6I, 6J, and S6D–S6F).

Next, the total amount of glutamate release from a single astrocyte was estimated based on the experimental values of sniffer-patch recording by using a diffusion model to fit the experimental measurements. The model was optimized to

consider the geometrical constraints of sniffer patch and to capture the diffused-away glutamate molecules that the sensor failed to detect (Figure 7A, see Extended Experimental Procedures). We calculated that one typical astrocyte releases 0.34 fmol of glutamate during the fast mode and 1.35 fmol during the slow mode (Figures 7B and 7C). These values could be compared to 2.64 fmol for the mechanical stimulation-induced glutamate release at the peak of response (Figures 7B and 7D). These estimations are comparable to the previously reported estimations (0.078–0.2 fmol by glutamate imaging [Domercq et al., 2006] and 3 fmol by HPLC [Takano et al., 2005]).

Using the same diffusion model, we simulated glutamate release from the point sources uniformly distributed on the astrocytic membrane and predicted the concentration of glutamate from 10 to 40 nm away from the neuronal membrane to mimic the astrocyte-neuron interaction (Figures 7H and 7I). Because the cytosolic glutamate concentration in astrocytes is as high as 2–10 mM (Ye et al., 2003), glutamate is assumed to flow out, down the gradient when TREK-1 and Best1 channels open. The simulated glutamate concentration for the fast mode release via TREK-1 was ~100 μM (Figure 7E) at the target receptor of the apposing neuronal membrane, whereas for slow mode via Best1, the concentration was ~0.9 μM (Figure 7F). From these values, we can predict that the slow mode will preferentially activate neuronal NMDA receptors (NMDAR), whereas the fast mode will preferentially activate mGluR in addition to NMDAR, according to the reported concentration-response relationship for each glutamate receptor (Figure 7G).

Finally, we tested these predictions by performing slice patch clamp recordings from CA1 pyramidal neurons to detect PAR1-induced astrocytic glutamate release (Figure 7J). The released glutamate is detected as an NMDAR-mediated current in the presence of nominal external Mg^{2+} (5 μM). We found that TFLLR induced a small but significant NMDAR-mediated current (Figure 7K), which was almost completely eliminated in the Best1 knockout mice (Figure 7L). TREK-1-shRNA injected into Best1 knockout mice further reduced the small portion of remaining NMDAR-mediated current (Figure 7M). To test whether astrocytic or neuronal Best1 is mediating the glutamate release, we employed the cell-type-specific gene-silencing system that combines the GFAP-CreERT2 mice (astrocytic Cre) or CaMKII-Cre mice (neuronal Cre) with Cre-lox-regulated shRNA cassette (Lee et al., 2010; Ventura et al., 2004). We could also achieve temporal control of Cre expression in GFAP-CreERT2 mice by intraperitoneal injection of tamoxifen. Using this system, we found that Best1-shRNA significantly reduced TFLLR-induced glutamate release in the absence of tamoxifen (sunflower oil injection) in GFAP-CreERT2 mice or in CaMKII-Cre mice (Figure 7N), as compared to the scrambled shRNA control (Figure 7O). On the other hand, tamoxifen injection significantly rescued the TFLLR-induced NMDAR current in GFAP-CreERT2 mice (Figure 7O), indicating that astrocytic Best1 is responsible for the majority of TFLLR-induced glutamate release. To see whether TFLLR-induced current is a genuine NMDAR-mediated current, we performed similar recordings in the presence of 2 mM external Mg^{2+} and obtained instant I-V relationship upon voltage ramp ranging from −100mV to +20mV. The I-V relationship of TFLLR-induced current showed a typical V-shape that is a hallmark of Mg^{2+}-dependent NMDAR-mediated conductance (Figures 7P and 7R). This V-shaped I-V was eliminated by the treatment with APV, a blocker of NMDAR (Figures 7Q and 7R). Taken together, these results indicate that Best1-mediated astrocytic glutamate release targets neuronal postsynaptic NMDAR, whereas TREK-1-mediated release does not.

DISCUSSION

Our study answers the ongoing controversies about the astrocytic glutamate release mechanisms. Now we understand why many have reported the evidence for vesicular glutamate release from astrocytes. Many studies in the past used mechanical stimulation to induce glutamate release (Araque et al., 1998, 2000; Montana et al., 2004). Our study demonstrates the existence of both BoToxB-sensitive and channel-mediated releases; strong stimuli, such as mechanical stimulation, cause BoToxB-sensitive glutamate release, whereas GPCR activation leads to channel-mediated release. We also note the critical problems of using inhibitors of vesicular release such as Bafilomycin A1, Concanamycin A, and Tetanus toxin. These inhibitors actively remove the surface AMPA receptors, thus impairing the sensor for glutamate and obscuring the interpretation of the results. Furthermore, these inhibitors and BoToxB significantly reduced the surface expression of TREK-1 in heterologous expression system (Figures S7C and S7D) and Best1 channels in astrocytes (Figures S7E and S7F). Therefore, these inhibitors should be used with caution, and the past results should be reinterpreted.

Our electron microscopy results indicate that Best1 is preferentially located at the microdomains near synapses, whereas TREK-1 is preferentially located at the soma and processes, providing differential sources for fast glutamate release by TREK-1 away from the synapse and slow glutamate release by Best1 near the synapse. In the recent report by Agulhon et al. (2010), the authors used MrgA1 transgenic mice with astrocytic expression of exogenous MrgA1 receptor and showed a lack of effect upon activation of this receptor. The authors concluded that astrocytic Ca^{2+} had no effect on synaptic transmission and plasticity (Agulhon et al., 2010). This lack of effect could be due to an inappropriate targeting of the exogenously introduced MrgA1 receptor (a G_q-coupled GPCR), which should be targeted near Best1 channels in the distal microdomains for proper release and function. In contrast to the exogenous MrgA1, we demonstrate that the activation of endogenous PAR1 releases Ca^{2+}-dependent astrocytic glutamate via Best1 channel and subsequently activates neuronal NMDAR.

Furthermore, our study demonstrates that glutamate release upon receptor activation is mostly due to channel-mediated release (Figure 6K), which is in line with the recent review by Hamilton and Attwell (2010) and other previous reports suggesting anion-channel-mediated release but without identifying the molecular identity of the channel (Li et al., 2012; Takano et al., 2005). We determined the molecular identity of the fast mode as TREK-1 and the slow mode as Best1 channel. We previously reported that tonic GABA release is mediated by Best1 in cerebellar astrocytes (Lee et al., 2010). We subsequently reported that astrocytes of CA1 hippocampus do not contain GABA, and thus there is very little tonic GABA release detected from

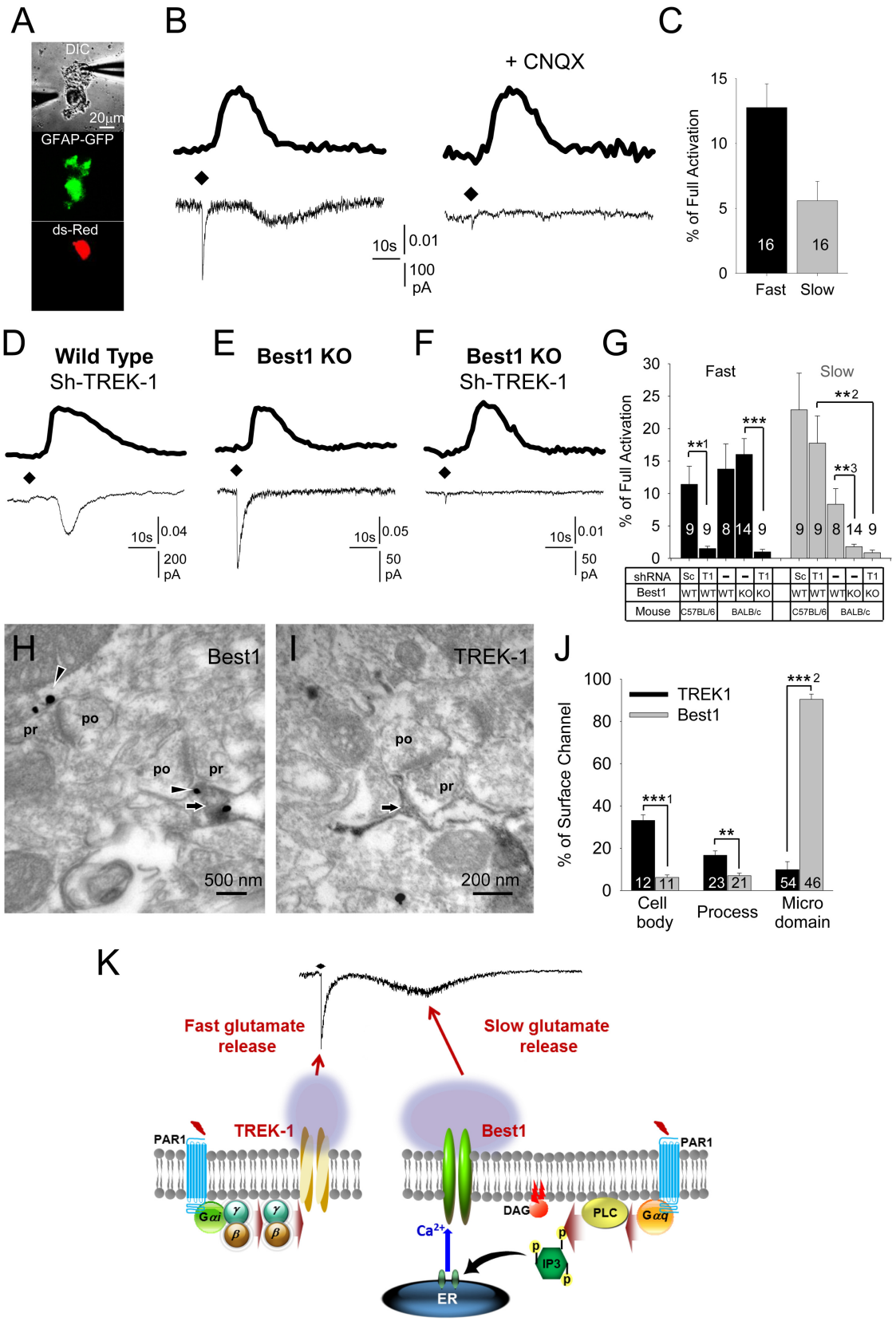
A
DIC
20μm
GFAP-GFP
ds-Red
B
+ CNQX
10s
0.01
100
pA
C
% of Full Activation
15
10
5
0
16
16
Fast
Slow
D
Wild Type
Sh-TREK-1
10s
0.04
200
pA
E
Best1 KO
10s
0.05
50
pA
F
Best1 KO
Sh-TREK-1
10s
0.01
50
pA
G
Fast
Slow
% of Full Activation
30
25
20
15
10
5
0
**1
***
**2
**3
9 9 8 14 9
9 9 8 14 9
shRNA Sc T1 – – T1 Sc T1 – – T1
Best1 WT WT WT KO KO WT WT WT KO KO
Mouse C57BL/6 BALB/c C57BL/6 BALB/c
H
Best1
pr
po
po
pr
500 nm
I
TREK-1
po
pr
200 nm
J
% of Surface Channel
100
80
60
40
20
0
TREK1
Best1
***1
**
***2
12 11
23 21
54 46
Cell body
Process
Micro domain
K
Fast glutamate release
Slow glutamate release
PAR1
TREK-1
Best1
PAR1
Gαi
γ
β
DAG
PLC
Gαq
Ca2+
IP3
p
ER

CA1 pyramidal neurons (Yoon et al., 2011). Although Best1 is permeable to both glutamate and GABA, it should mediate glutamate release from hippocampal astrocytes because they do not contain GABA. In addition, our study demonstrates that, when a G_i-coupled GPCR ($GABA_B$, CB1, or A1R) is activated, there is a concurrent induction of Ca^{2+}-independent glutamate release that is linked to G_i activation, dissociation of $G_{\beta\gamma}$, binding of $G_{\beta\gamma}$ to N terminus of TREK-1, and opening of TREK-1 channel.

Finally, we demonstrate the ability of a K2P channel permeating and releasing glutamate upon binding of $G_{\beta\gamma}$. There have been only few channels that directly interact with $G_{\beta\gamma}$. These include GIRK (Huang et al., 1995) and alpha subunits of some voltage-gated Ca^{2+} channels (Li et al., 2005). The K2P channel is a new member of the family of channels that show direct interaction with $G_{\beta\gamma}$. The remarkable ability of a potassium-permeable channel to dilate its pore to permeate large molecules such as glutamate is quite interesting. Pore dilation is a rare phenomenon that has been observed with few ion channels, such as TRPV1 (Binshtok et al., 2007) and P2X7 (Virginio et al., 1999). A detailed structural analysis should give us new insights on how pore dilation in TREK-1 can occur upon the binding of $G_{\beta\gamma}$.

In conclusion, astrocytes display multiple routes of glutamate release, each with a unique molecular mechanism, specific timescale, differential location, and different neuronal target receptor. Such diversity teaches us that astrocytes, once a neglected brain cell type, are emerging as an important source of glutamate, which can potentially influence neuronal excitability under various physiological as well as pathological conditions.

EXPERIMENTAL PROCEDURES

Sniffer-Patch Technique

Sniffer patch was composed of Fura-2 imaging for Ca^{2+} from astrocytes and current recording from HEK293T cells expressing GluR1-L497Y. To release glutamate from astrocyte, PAR-1 was activated by pressure application of TFLLR peptide. On the day of experiment, cultured mouse astrocytes (HEK293T cells added) were incubated with 5 μM Fura-2 AM (mixed with 5 μl of 20% Pluronic acid) (Invitrogen) for 40 min, washed at room temperature, and subsequently transferred to the microscope stage for imaging. External solution contained (in mM): 150 NaCl, 10 HEPES, 3 KCl, 2 $CaCl_2$, 2 $MgCl_2$, and 5.5 glucose (pH adjusted to pH 7.3 and osmolarity adjusted to 325 mOsmol kg^{-1}). Intensity images of 510 nm wavelength were taken at 340 nm and 380 nm excitation wavelengths by using iXon EMCCD (ANDOR). Two resulting images were used for ratio calculations in Imaging Workbench version 6.2 (Indec Systems). GluR1L497Y-mediated currents were recorded from HEK293T cells under voltage clamp (V_h = –70mV) using Multiclamp 700B amplifier acquired with pClamp 9.2 (Molecular Devices). Recording electrodes (4–7MΩ) were filled with (mM): 110 Cs-Gluconate, 30 CsCl, 0.5 $CaCl_2$, 10 HEPES, 4 Mg-ATP, 0.3 Na3-GTP, and 10 BAPTA (pH adjusted to 7.3 with CsOH and osmolarity adjusted to 290–310 mOsm/kg with sucrose). For simultaneous recording, Imaging Workbench was synchronized with pClamp 9.2.

To study G_i pathway, Pertussis toxin, pCDNA3.1-SS-ECFP-TM-Gi1-CG (GiCG), and pCDNA3.1-SS-ECFP-TM-Gs were used. To study the dissociation of G_i-$G_{\beta\gamma}$ pathway, pRK-β-Ark-C terminus, pIRES2-dsRED-Phosducin-C terminus, and specific G_i agonists (Baclofen for $GABA_B$, CCPA for adenosine receptor 1, and ACEA for Cannabinoid receptor) were used. To study G_q pathway, BAPTA-AM and pSPORT6-RGS-2 were used. To inhibit vesicular release, Botulinum toxin was injected with impermeable Fura-2 to a single astrocyte. To inhibit anion channels, NPPB, NFA, DIDS, and quinine were used. To test whether glutamate release involved TREK-1, pSicoR-TREK-1-shRNA to gene-silence TREK-1 expression and pIRES2-GFP-TREK-1(rat) for the rescue experiment were used. To test whether glutamate release involves Best1, pSicoR-Best1-shRNA for blocking Best1 expression and pSicoR-Best1-shRNA and pIRES2-dsRed-Best1 (shRNA-insensitive form) for rescue experiment were used.

Two-Cell Sniffer Patch

Upon membrane rupture, currents were recorded from astrocyte under voltage clamp (V_h = –70mV). Recording electrodes (4–7MΩ) were filled with (mM): 5 glutamate, 135 CsCl, 0.5 $CaCl_2$, 10 HEPES, 4 Mg-ATP, 0.3 Na3-GTP, 10 BAPTA, and 6.09 nM $G_{\beta\gamma}$ (pH adjusted to 7.3 with CsOH and osmolarity adjusted to 290–310 mOsm/kg with sucrose). In the competitive peptide assay, 100 μM N1-4 synthesized peptides were added to patch pipette and injected into astrocyte. GluR1L497Y-mediated currents were recorded from HEK293T cells under voltage clamp (V_h = –70mV). Recording electrodes (4–7 MΩ) were filled with (mM): 110 Cs-Gluconate, 30 CsCl, 0.5 $CaCl_2$, 10 HEPES, 4 Mg-ATP, 0.3 Na3-GTP, and 10 BAPTA (pH adjusted to 7.3 with CsOH and osmolarity adjusted to 290–310 mOsm/kg with sucrose). Purified bovine $G_{\beta\gamma}$ (Calbiochem 371768) was injected into astrocyte, and the current amplitude was measured 10 min after membrane rupture.

Biochemical Evidence for Interaction of TREK-1 and G_γ

The binding partners of N terminus of TREK-1 were screened by yeast two-hybrid system (Y2H) (Kim et al., 2010). The binding site of TREK-1 on GNG4 was identified by Y2H and was confirmed by MBP pull-down assay and coimmunoprecipitation. The binding domain of GNG4 on TREK-1 was

Figure 6. TREK-1 and Best1 Mediate Fast and Slow Glutamate Release in Acutely Dissociated Astrocytes and Show Differential Localization in CA1 Hippocampal Astrocytes

(A) DIC, GFP (astrocyte), and ds-Red (sensor cell) images for sniffer patch from acutely dissociated CA1 hippocampal astrocyte prepared from adult GFAP-GFP mouse.

(B) Sensor current traces from one astrocyte before and during 10 μM CNQX.

(C) Summary bar graph.

(D) Traces for TREK-1-shRNA-expressing astrocyte.

(E) Trace for Best1 knockout (KO) mouse.

(F) Trace for Best1 KO mouse expressing TREK-1-shRNA.

(G) Summary bar graph (**1, p = 0.002; **2, p = 0.001; **3, p = 0.002; and ***p = 0.0008).

(H and I) Electron microscopic immunostaining for Best1 (H) and TREK-1 (I) combined with immunostaining for GFP in hippocampal CA1 of GFAP-GFP mouse. Best1 and TREK-1 are stained with immunogold with silver enhancement (dark specks, arrowheads), and GFP is stained with immunoperoxidase (dark amorphous deposits, arrows). Pr, presynapse; Po, postsynapse.

(J) Summary graph for percentage (%) of gold particles for TREK-1 and Best1 located on the plasma membrane of cell body, process, and microdomain (***1, p = 0.0005; **p = 0.008; ***2, p = 0.0001).

(K) Molecular model of receptor-mediated glutamate release in astrocyte. Upon PAR-1 activation, dissociated $G_{\beta\gamma}$ activates TREK-1 to induce fast mode of glutamate release, whereas $G_{\alpha q}$-mediated signaling and Ca^{2+} induce slow mode of Best1-mediated glutamate release.

All values are expressed as mean ±SEM. See also Figure S6.

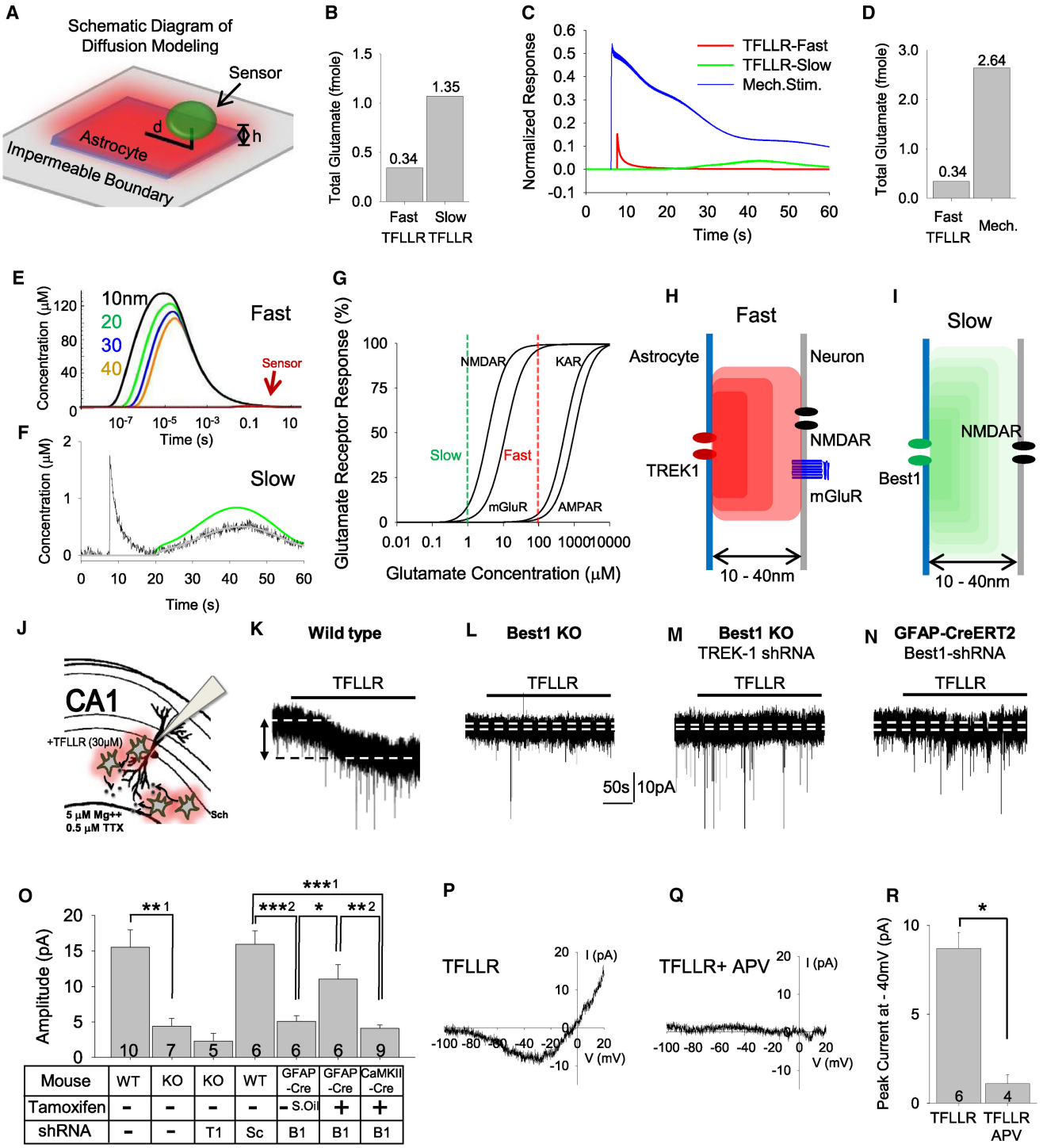

Figure 7. Diffusion Modeling Predicts the Concentrations of Fast and Slow Modes and Their Target Neuronal Receptors: Confirmation by Slice Whole-Cell Recording

(A) The schematic diagram of the diffusion model simulation. Geometry of a single astrocyte on an impermeable boundary is modeled by a square of 100 μm × 100 μm.

(B) Based on the normalized electrical responses captured by the sensor (HEK293T cell), the original release of glutamate from the astrocyte was estimated. According to the reconstructed release, the normalized responses are calculated. The release by TFLLR stimulation is divided into two modes of the leading transient (fast) followed by the smooth (slow).

(C) According to the simulation result, fast and slow modes release about 0.34 fmol and 1.35 fmol, respectively. Peak of fast mode is higher than that of slow mode, but slow mode continuously releases glutamate in comparison to fast mode where an instantaneous release occurs.

determined by coimmunoprecipitation after expressing N or C terminus of GNG4 in HEK293T cells, together with full-length TREK-1.

SUPPLEMENTAL INFORMATION

Supplemental Information includes Extended Experimental Procedures, seven figures, and one table and can be found with this article online at http://dx.doi.org/10.1016/j.cell.2012.09.005.

ACKNOWLEDGMENTS

This work was supported by the World Class Institute (WCI 2009-003), MRC (2012-0000305), and Basic Science Research (2010-0029460) Programs of the NRF funded by the MEST of Korea and also by NIH (R01-EY013160) and a grant from Research to Prevent Blindness to the Department of Ophthalmology and Vision Science at the University of Arizona. We thank George Augustine, Larry Cohen, and Keiko Tanaka for careful editing of the manuscript. We thank Taekeun Kim for technical support for immunocytochemistry, Nammi Park for technical support for Y2H, Lucie Langevin for providing clone of pRK-β-Ark-C terminus, and Nevin A. Lambert for pCDNA3.1-SS-ECFP-TM-Gi1-CG (GiCG) and pCDNA3.1-SS-ECFP-TM-Gs.

Received: April 4, 2012
Revised: June 18, 2012
Accepted: September 5, 2012
Published: September 27, 2012

REFERENCES

Agulhon, C., Fiacco, T.A., and McCarthy, K.D. (2010). Hippocampal short- and long-term plasticity are not modulated by astrocyte Ca2+ signaling. Science *327*, 1250–1254.

Araque, A., Sanzgiri, R.P., Parpura, V., and Haydon, P.G. (1998). Calcium elevation in astrocytes causes an NMDA receptor-dependent increase in the frequency of miniature synaptic currents in cultured hippocampal neurons. J. Neurosci. *18*, 6822–6829.

Araque, A., Li, N., Doyle, R.T., and Haydon, P.G. (2000). SNARE protein-dependent glutamate release from astrocytes. J. Neurosci. *20*, 666–673.

Bekkers, J.M., and Stevens, C.F. (1995). Quantal analysis of EPSCs recorded from small numbers of synapses in hippocampal cultures. J. Neurophysiol. *73*, 1145–1156.

Bezzi, P., Gundersen, V., Galbete, J.L., Seifert, G., Steinhäuser, C., Pilati, E., and Volterra, A. (2004). Astrocytes contain a vesicular compartment that is competent for regulated exocytosis of glutamate. Nat. Neurosci. *7*, 613–620.

Binshtok, A.M., Bean, B.P., and Woolf, C.J. (2007). Inhibition of nociceptors by TRPV1-mediated entry of impermeant sodium channel blockers. Nature *449*, 607–610.

Blüml, K., Schnepp, W., Schröder, S., Beyermann, M., Macias, M., Oschkinat, H., and Lohse, M.J. (1997). A small region in phosducin inhibits G-protein betagamma-subunit function. EMBO J. *16*, 4908–4915.

Brenner, T., and O'Shaughnessy, K.M. (2008). Both TASK-3 and TREK-1 two-pore loop K channels are expressed in H295R cells and modulate their membrane potential and aldosterone secretion. Am. J. Physiol. Endocrinol. Metab. *295*, E1480–E1486.

Cavelier, P., and Attwell, D. (2005). Tonic release of glutamate by a DIDS-sensitive mechanism in rat hippocampal slices. J. Physiol. *564*, 397–410.

Clapham, D.E. (2007). Calcium signaling. Cell *131*, 1047–1058.

Clements, J.D., Lester, R.A., Tong, G., Jahr, C.E., and Westbrook, G.L. (1992). The time course of glutamate in the synaptic cleft. Science *258*, 1498–1501.

Digby, G.J., Sethi, P.R., and Lambert, N.A. (2008). Differential dissociation of G protein heterotrimers. J. Physiol. *586*, 3325–3335.

Domercq, M., Brambilla, L., Pilati, E., Marchaland, J., Volterra, A., and Bezzi, P. (2006). P2Y1 receptor-evoked glutamate exocytosis from astrocytes: control by tumor necrosis factor-alpha and prostaglandins. J. Biol. Chem. *281*, 30684–30696.

Farinelli, S.E., and Nicklas, W.J. (1992). Glutamate metabolism in rat cortical astrocyte cultures. J. Neurochem. *58*, 1905–1915.

Fiacco, T.A., and McCarthy, K.D. (2004). Intracellular astrocyte calcium waves in situ increase the frequency of spontaneous AMPA receptor currents in CA1 pyramidal neurons. J. Neurosci. *24*, 722–732.

Greenwood, I.A., and Leblanc, N. (2007). Overlapping pharmacology of Ca2+-activated Cl- and K+ channels. Trends Pharmacol. Sci. *28*, 1–5.

Grosche, J., Matyash, V., Möller, T., Verkhratsky, A., Reichenbach, A., and Kettenmann, H. (1999). Microdomains for neuron-glia interaction: parallel fiber signaling to Bergmann glial cells. Nat. Neurosci. *2*, 139–143.

Halassa, M.M., Fellin, T., and Haydon, P.G. (2007). The tripartite synapse: roles for gliotransmission in health and disease. Trends Mol. Med. *13*, 54–63.

Hamilton, N.B., and Attwell, D. (2010). Do astrocytes really exocytose neurotransmitters? Nat. Rev. Neurosci. *11*, 227–238.

Haydon, P.G., and Carmignoto, G. (2006). Astrocyte control of synaptic transmission and neurovascular coupling. Physiol. Rev. *86*, 1009–1031.

(D) Glutamate releases are 0.34 fmol for fast mode of TFLLR as in (C) and 2.64 fmol for mechanical stimulation.
(E) The glutamate concentration profiles of fast mode are estimated at positions apart from the center of the astrocyte by 10 to 40 nm as in (H) to mimic the distance between the astrocyte and the counter receptors in neighboring neuron.
(F) In the case of slow mode, the glutamate concentration profiles are similar with respect to the gaps of 10 to 40 nm.
(G) Fast mode is easily detectable by NMDAR and mGluR, whereas slow mode is detectable only by NMDAR.
(H) Schematic diagram for fast mode.
(I) Schematic diagram for slow mode.
(J) Experimental schematic diagram for whole-cell patch clamp to measure astrocytic glutamate-induced neuronal responses. To observe NMDAR-dependent whole-cell current from CA1 pyramidal neuron, Mg^{2+}-free (~5 μM) ACSF with TTX (0.5 μM) was used. To induce Ca^{2+}-dependent glutamate release from astrocytes, PAR1 agonist (TFLLR; 30 μM) was treated in bath.
(K–N) Traces from CA1 pyramidal neuron in wild-type (K) or shRNA-expressing mice (N). The arrow and dotted lines indicate the current measurement before and after TFLLR treatment.
(O) Summary bar graph showing averaged astrocytic glutamate-induced whole-cell current from CA1 neuron. KO, Best1 knockout mouse. GFAP-Cre, GFAP-CreERT2 mouse. CaMKII-Cre, CaMKII-Cre mouse. Sc, scrambled shRNA. B1, Best1-shRNA. -, without tamoxifen injection (S.Oil, sunflower-oil-injected control). +, with tamoxifen injection. **1, p = 0.002; **2, p = 0.001; ***1, p = 0.00007; ***2, p = 0.00004; *p = 0.022. Numbers of tested slices from at least three independent mice is indicated on each bar.
(P) Subtracted trace between I-V curve from CA1 neuron treated with TFLLR and I-V curve from CA1 neuron posttreated with APV to isolate NMDAR activation.
(Q) Subtracted trace between I-V curve from CA1 neuron pretreated with APV and with TFLLR.
(R) Summary graph for peak current at −40mV (*p = 0.02).
All values are mean ±SEM. See also Figures S7A and S7B.

Heximer, S.P., Watson, N., Linder, M.E., Blumer, K.J., and Hepler, J.R. (1997). RGS2/G0S8 is a selective inhibitor of Gqalpha function. Proc. Natl. Acad. Sci. USA *94*, 14389–14393.

Hollenberg, M.D., Saifeddine, M., al-Ani, B., and Kawabata, A. (1997). Proteinase-activated receptors: structural requirements for activity, receptor cross-reactivity, and receptor selectivity of receptor-activating peptides. Can. J. Physiol. Pharmacol. *75*, 832–841.

Huang, C.L., Slesinger, P.A., Casey, P.J., Jan, Y.N., and Jan, L.Y. (1995). Evidence that direct binding of G beta gamma to the GIRK1 G protein-gated inwardly rectifying K+ channel is important for channel activation. Neuron *15*, 1133–1143.

Innocenti, B., Parpura, V., and Haydon, P.G. (2000). Imaging extracellular waves of glutamate during calcium signaling in cultured astrocytes. J. Neurosci. *20*, 1800–1808.

Jourdain, P., Bergersen, L.H., Bhaukaurally, K., Bezzi, P., Santello, M., Domercq, M., Matute, C., Tonello, F., Gundersen, V., and Volterra, A. (2007). Glutamate exocytosis from astrocytes controls synaptic strength. Nat. Neurosci. *10*, 331–339.

Junge, C.E., Lee, C.J., Hubbard, K.B., Zhang, Z., Olson, J.J., Hepler, J.R., Brat, D.J., and Traynelis, S.F. (2004). Protease-activated receptor-1 in human brain: localization and functional expression in astrocytes. Exp. Neurol. *188*, 94–103.

Kang, J., Jiang, L., Goldman, S.A., and Nedergaard, M. (1998). Astrocyte-mediated potentiation of inhibitory synaptic transmission. Nat. Neurosci. *1*, 683–692.

Kim, E., Hwang, E.M., Yarishkin, O., Yoo, J.C., Kim, D., Park, N., Cho, M., Lee, Y.S., Sun, C.H., Yi, G.S., et al. (2010). Enhancement of TREK1 channel surface expression by protein-protein interaction with beta-COP. Biochem. Biophys. Res. Commun. *395*, 244–250.

Koch, W.J., Inglese, J., Stone, W.C., and Lefkowitz, R.J. (1993). The binding site for the beta gamma subunits of heterotrimeric G proteins on the beta-adrenergic receptor kinase. J. Biol. Chem. *268*, 8256–8260.

Lee, C.J., Mannaioni, G., Yuan, H., Woo, D.H., Gingrich, M.B., and Traynelis, S.F. (2007). Astrocytic control of synaptic NMDA receptors. J. Physiol. *581*, 1057–1081.

Lee, S., Yoon, B.E., Berglund, K., Oh, S.J., Park, H., Shin, H.S., Augustine, G.J., and Lee, C.J. (2010). Channel-mediated tonic GABA release from glia. Science *330*, 790–796.

Li, X., Hümmer, A., Han, J., Xie, M., Melnik-Martinez, K., Moreno, R.L., Buck, M., Mark, M.D., and Herlitze, S. (2005). G protein beta2 subunit-derived peptides for inhibition and induction of G protein pathways. Examination of voltage-gated Ca2+ and G protein inwardly rectifying K+ channels. J. Biol. Chem. *280*, 23945–23959.

Li, D., Hérault, K., Isacoff, E.Y., Oheim, M., and Ropert, N. (2012). Optogenetic activation of LiGluR-expressing astrocytes evokes anion channel-mediated glutamate release. J. Physiol. *590*, 855–873.

Macfarlane, S.R., Seatter, M.J., Kanke, T., Hunter, G.D., and Plevin, R. (2001). Proteinase-activated receptors. Pharmacol. Rev. *53*, 245–282.

Marmorstein, L.Y., Wu, J., McLaughlin, P., Yocom, J., Karl, M.O., Neussert, R., Wimmers, S., Stanton, J.B., Gregg, R.G., Strauss, O., et al. (2006). The light peak of the electroretinogram is dependent on voltage-gated calcium channels and antagonized by bestrophin (best-1). J. Gen. Physiol. *127*, 577–589.

Montana, V., Ni, Y., Sunjara, V., Hua, X., and Parpura, V. (2004). Vesicular glutamate transporter-dependent glutamate release from astrocytes. J. Neurosci. *24*, 2633–2642.

Nedergaard, M., Takano, T., and Hansen, A.J. (2002). Beyond the role of glutamate as a neurotransmitter. Nat. Rev. Neurosci. *3*, 748–755.

O'Driscoll, K.E., Leblanc, N., Hatton, W.J., and Britton, F.C. (2009). Functional properties of murine bestrophin 1 channel. Biochem. Biophys. Res. Commun. *384*, 476–481.

Obrenovitch, T.P., and Zilkha, E. (2001). Microdialysis coupled to online enzymatic assays. Methods *23*, 63–71.

Park, H., Oh, S.J., Han, K.S., Woo, D.H., Park, H., Mannaioni, G., Traynelis, S.F., and Lee, C.J. (2009). Bestrophin-1 encodes for the Ca2+-activated anion channel in hippocampal astrocytes. J. Neurosci. *29*, 13063–13073.

Parpura, V., and Haydon, P.G. (2000). Physiological astrocytic calcium levels stimulate glutamate release to modulate adjacent neurons. Proc. Natl. Acad. Sci. USA *97*, 8629–8634.

Parpura, V., Basarsky, T.A., Liu, F., Jeftinija, K., Jeftinija, S., and Haydon, P.G. (1994). Glutamate-mediated astrocyte-neuron signalling. Nature *369*, 744–747.

Sorensen, S.D., Nicole, O., Peavy, R.D., Montoya, L.M., Lee, C.J., Murphy, T.J., Traynelis, S.F., and Hepler, J.R. (2003). Common signaling pathways link activation of murine PAR-1, LPA, and S1P receptors to proliferation of astrocytes. Mol. Pharmacol. *64*, 1199–1209.

Takano, T., Kang, J., Jaiswal, J.K., Simon, S.M., Lin, J.H., Yu, Y., Li, Y., Yang, J., Dienel, G., Zielke, H.R., and Nedergaard, M. (2005). Receptor-mediated glutamate release from volume sensitive channels in astrocytes. Proc. Natl. Acad. Sci. USA *102*, 16466–16471.

Traynelis, S.F., Wollmuth, L.P., McBain, C.J., Menniti, F.S., Vance, K.M., Ogden, K.K., Hansen, K.B., Yuan, H., Myers, S.J., and Dingledine, R. (2010). Glutamate receptor ion channels: structure, regulation, and function. Pharmacol. Rev. *62*, 405–496.

Ventura, A., Meissner, A., Dillon, C.P., McManus, M., Sharp, P.A., Van Parijs, L., Jaenisch, R., and Jacks, T. (2004). Cre-lox-regulated conditional RNA interference from transgenes. Proc. Natl. Acad. Sci. USA *101*, 10380–10385.

Virginio, C., MacKenzie, A., Rassendren, F.A., North, R.A., and Surprenant, A. (1999). Pore dilation of neuronal P2X receptor channels. Nat. Neurosci. *2*, 315–321.

Wang, H.S., Dixon, J.E., and McKinnon, D. (1997). Unexpected and differential effects of Cl- channel blockers on the Kv4.3 and Kv4.2 K+ channels. Implications for the study of the I(to2) current. Circ. Res. *81*, 711–718.

West, R.E., Jr., Moss, J., Vaughan, M., Liu, T., and Liu, T.Y. (1985). Pertussis toxin-catalyzed ADP-ribosylation of transducin. Cysteine 347 is the ADP-ribose acceptor site. J. Biol. Chem. *260*, 14428–14430.

Ye, Z.C., Wyeth, M.S., Baltan-Tekkok, S., and Ransom, B.R. (2003). Functional hemichannels in astrocytes: a novel mechanism of glutamate release. J. Neurosci. *23*, 3588–3596.

Yoon, B.E., Jo, S., Woo, J., Lee, J.H., Kim, T., Kim, D., and Lee, C.J. (2011). The amount of astrocytic GABA positively correlates with the degree of tonic inhibition in hippocampal CA1 and cerebellum. Mol. Brain *4*, 42.

Zhang, Y., Stanton, J.B., Wu, J., Yu, K., Hartzell, H.C., Peachey, N.S., Marmorstein, L.Y., and Marmorstein, A.D. (2010). Suppression of Ca2+ signaling in a mouse model of Best disease. Hum. Mol. Genet. *19*, 1108–1118.

Zhou, M., Xu, G., Xie, M., Zhang, X., Schools, G.P., Ma, L., Kimelberg, H.K., and Chen, H. (2009). TWIK-1 and TREK-1 are potassium channels contributing significantly to astrocyte passive conductance in rat hippocampal slices. J. Neurosci. *29*, 8551–8564.